



Deposited via The University of Sheffield.

White Rose Research Online URL for this paper:

<https://eprints.whiterose.ac.uk/id/eprint/77699/>

Version: Accepted Version

Article:

Melcher, J., Champneys, A.R. and Wagg, D.J. (2013) The impacting cantilever: modal non-convergence and the importance of stiffness matching. *Philosophical Transactions of The Royal Society A Mathematical, Physical and Engineering Sciences*, 371 (1993). 20120434. - . ISSN: 1364-503X

<https://doi.org/10.1098/rsta.2012.0434>

Reuse

Items deposited in White Rose Research Online are protected by copyright, with all rights reserved unless indicated otherwise. They may be downloaded and/or printed for private study, or other acts as permitted by national copyright laws. The publisher or other rights holders may allow further reproduction and re-use of the full text version. This is indicated by the licence information on the White Rose Research Online record for the item.

Takedown

If you consider content in White Rose Research Online to be in breach of UK law, please notify us by emailing eprints@whiterose.ac.uk including the URL of the record and the reason for the withdrawal request.

The impacting cantilever: modal non-convergence and the importance of stiffness matching

John T. Melcher, Alan R. Champneys*, David J. Wagg
Departments of Engineering Mathematics and Mechanical Engineering,
Queen's Building, University of Bristol, Bristol BS8 1TR

Citation: Philosophical Transactions of the Royal Society A:
Mathematical, Physical and Engineering Sciences
371(1993):1471–2962, 2013.
doi:10.1098/rsta.2012.0434

Abstract

The problem of an Euler-Bernoulli cantilever beam whose free end impacts with a point constraint is revisited from the point of view of modal analysis. It is shown that there is non-uniqueness of consistent impact laws for a given modal truncation. Moreover, taking an N -mode compliant, bilinear formulation and passing to the rigid limit leads to a sequence of impact models that does not converge as $N \rightarrow \infty$. The dynamics of such truncated models are studied numerically and found to give rise to quite different dynamics depending on the number of degrees of freedom taken. The simulations are compared with results from simple experiments which show a propensity for multiple-tap dynamics, in which higher-order modes lead to rapidly cycling intermittent contact. The conclusion reached is that to derive an accurate model one needs to avoid the impact limit altogether, and take sufficiently many modes in the formulation to match the actual stiffness of the constraining stop.

1 Introduction

Mechanical systems with repeated impacts arise in a wide variety of applications. Examples include atomic force microscopy (AFM), radio-frequency

*Corresponding author: a.r.champneys@bristol.ac.uk

switches, Braille printers, impact forging, percussive moling, backlash in gears, freeplay in control surfaces and numerous vibro-impact problems involving buzz, squeak and rattle. See for example [4, 2] for general theory and numerous examples. A particular motivation for this work is an attempt to understand the complex dynamical properties of tapping mode AFM as observed, e.g. in [14, 17, 30, 20, 9]. Here, a flexible micro-scale cantilever is excited at its clamped end so that a narrow tip at the free end can repeatedly impact with a sample in order to capture surface properties. Fundamental questions arise as to what is the “correct” rational-mechanics formulation of the impact of a continuously flexible structure in order to faithfully capture its post-impact dynamics.

A commonly used formalism is that of rigid-body mechanics in which impact is instantaneous and lossy, with the energy dissipation being captured by a Newtonian coefficient of restitution. The study of such single-degree-of-freedom, impact oscillators goes back to the Eastern European literature beginning in the 1950s, see e.g. [6, 1] and references therein, culminating in the work of Peterka in the 1970s [15]. The theory was rediscovered in the West a decade or so later through the work of Shaw & Holmes [19] and by Michael Thompson, to whom this volume is dedicated, together with his student Ghaffari [22]. Much information is now understood about the influence of grazing and chattering on the global dynamics, see e.g. [3] and [4, Ch.1] for reviews.

Experimental investigation of impact oscillators at the macro scale, has shown qualitative agreement with the theory, see e.g. [16, 29, 5, 13, 23] (the latter being a different Michael Thompson, albeit a former PhD student from the *same* UCL group!) However, precise quantitative agreement is hampered by the fact that Newtonian restitution is a gross approximation to the true process of energy dissipation. In reality, dissipation occurs through excitation of internal degrees of freedom of the objects undergoing impact. In the case of a clamped cantilever undergoing intermittent contact at its free end, this problem is particularly acute because of the propensity of each impact to excite higher-order modes of the structure.

Turning to tapping mode AFM, an often adopted modality is that of dynamic force spectroscopy in which the cantilever’s deflection is used as a proxy for the interaction force between the tip and the sample. Then, using a model-based approach, the signal is inverted to reconstruct the tip-sample force as a function of the tip displacement, see e.g. [20, 24] and references therein. Material properties of the sample, e.g. its stiffness, viscosity, etc., can then in theory be inferred from the data by fitting the reconstructed, tip-sample forces to a model. Although such a model-based inversion technique

can be used to capture single coefficients like that of Newtonian restitution, such an approach typically does not take into account the response of higher modes of the cantilever beam. Such higher modes can cause multiple-tap dynamics, where a single impact is followed by several others [9] like a drummer's stick during a drum roll. Such dynamic behaviour and the question of how to model it, is the chief motivation for this paper.

To be concrete, we shall consider the problem of a cantilever that is subject to spatially distributed forcing and either viscous or material damping, whose free end is allowed to make point contact with a stiff constraint. The central question is how to faithfully model such a situation using finite-dimensional impact mechanics. In particular, in such problems one often appeals to two separate limiting processes to derive a tractable reduced-order mathematical model for such a configuration. The first process is that of taking the infinite stiffness limit, to avoid the numerical problems associated with different time scales of contact and free motion. Indeed, in the single-degree-of-freedom case Nordmark [11] has shown theoretically and via simulation that the dynamics of a bilinear oscillator converges to that of the corresponding impact oscillator in the limit that one stiffness becomes infinite. The second limiting process is modal truncation. For a linear beam, a finite collection of modes can capture the response exactly, provided the forcing is entirely within the subspace spanned by those modes. But impact introduces strong nonlinearity, of a distributional kind, and one cannot appeal to such standard modal convergence theorems.

The rest of this paper is organised as follows. §2 introduces the model configuration to be studied. It is shown how, given a compliant constraint, modal decomposition and Galerkin projection can be used to formulate a reduced-order model up to any order. §3 goes on to study the same model in the rigid impact limit, with a given coefficient r . Two proposed methods from the literature for posing an impact law for a given order modal truncation are presented. §4 then revisits such impact laws by taking a succession of truncated models from §3 and passing to the large stiffness limit. It is shown that this process does not converge. In §5 it is shown via numerical simulation that the observed dynamics of these impacting N -mode truncations depend strongly on the choice of N . §6 then presents experimental results for an impacting cantilever and shows how to optimally capture the observations using reduced order models. Finally, §7 draws conclusions and considers practical implications for AFM operation.

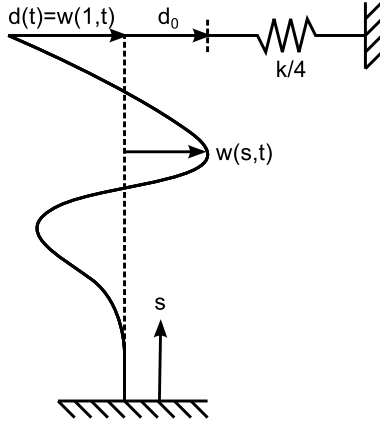


Figure 1: Definition sketch of the physical system. The transverse deflection is $w(s, t)$ of the cantilever where s is the axial displacement from the fixed-end. At the free-end ($s = 1$) the cantilever is constrained by a compliant stop with stiffness $k/4$ for $w(1, t) = d(t) > d_0$.

2 Beam with compliant constraint

In this section and the next two we shall undertake a theoretical analysis of a cantilever beam with an isolated point impact. As is common in the literature we shall make several simplifying assumptions, in particular that damping occurs only through viscous drag and that impact occurs precisely at the end of the cantilever. In the simulations in §5 below, we shall relax the former assumption and include material damping, in order to get a better match with the experimental results in §6. The theory is, in principle, unaffected by more complex damping models or more general impact positions but becomes rather cumbersome to present due to modal coupling and lack of explicit solutions.

2.1 Continuum model

Consider a uniform, Euler-Bernoulli cantilever beam with proportional damping, spatially extended external forcing and end contact with a compliant stop, see Fig. 1. Under the usual assumptions of beam theory, after an appropriate rescaling of space and time, its dynamics can be represented by

the dimensionless equation

$$\begin{aligned}
w_{tt}(s, t) + 2\alpha w_t(s, t) + w_{ssss}(s, t) &= f(s, t) \\
s = 0: \quad w = w_s &= 0 \\
s = 1: \quad w_{ss} = 0, \quad w_{sss} &= \begin{cases} 0, & w \leq d_0 \\ \frac{k}{4}(d_0 - w), & w > d_0. \end{cases}
\end{aligned} \tag{1}$$

Here w is the scaled transverse deflection of the beam, $s \in [0, 1]$ is an axial co-ordinate, with $s = 0$ representing the clamped end and $s = 1$ the free end. Subscripts s or t on w denote partial differentiation with respect to that variable, 2α is a coefficient of mass-proportional viscous damping and $f(s, t)$ represents an axially-distributed, time-varying loading. Note that the beam's bending stiffness and mass density have both been scaled to unity in this formulation, without loss of generality. The presence of a compliant, one-sided amplitude constraint at the free-end of the cantilever is captured via the piecewise-linear shear boundary condition, where d_0 is the equilibrium distance between the free-end of the cantilever and the one-sided constraint, which (for convenience of later calculations) is assumed to have a scaled stiffness $k/4$.

The equation of motion (1) represents a piecewise-smooth boundary-value problem (BVP) that can be considered as a nonlinear dynamical system on an appropriate space of functions defined on the interval $[0, 1]$. The only nonlinearity is the Heaviside discontinuity in the boundary conditions that occurs when $w(1, t) = d_0$. But if we consider motion that does not cross this constraint, then (1) represents a linear, self-adjoint equation. In what follows we shall let the subscript $+$ denote the region $w(1, t) \geq d_0$ where the beam is constrained by the stop and $-$ denote the region $w(1, t) < d_0$ where the cantilever is unconstrained.

Natural frequencies for the unforced, undamped problem can be obtained in the $+$ and $-$ regions separately by restricting motion to the relevant region, setting $\alpha = f = 0$ in (1) and looking for solutions of the form $w(s, t) = \psi_i^\pm(s)e^{i\omega t}$. This produces a countably infinite set of mutually orthogonal eigenfunctions,

$$\psi_i^\pm(s) = \cos(\beta_i^\pm s) - \cosh(\beta_i^\pm s) - \sigma_i^\pm [\sin(\beta_i^\pm s) - \sinh(\beta_i^\pm s)], \tag{2}$$

where

$$\sigma_i^\pm = \frac{\cos \beta_i^\pm + \cosh \beta_i^\pm}{\sin \beta_i^\pm + \sinh \beta_i^\pm},$$

with β_i^\pm being the i th positive solution to

$$\cos \beta \cosh \beta + 1 + \frac{k^\pm}{4\beta^3} (\sin \beta \cosh \beta - \cos \beta \sinh \beta) = 0. \quad (3)$$

Here k^\pm is a bimodal stiffness, with $k^- = 0$ and $k^+ = k$, and $(\beta_i^\pm)^2$ represents the i th eigenfrequency of the linear problem.

In the expression (3) the terms inside and outside the parentheses correspond to the characteristic equations for the eigenfrequencies of a clamped-pinned beam and a simple cantilever beam, respectively. The factor $k/(4\beta^3)$ represents a weighting between the two characteristic equations. If $k \ll (\beta_i^-)^3$, then expanding the solution of (3) in the $+$ region for small values of k about β_i^- we find

$$(\beta_i^+)^4 = (\beta_i^-)^4 + k + \mathcal{O}(k^2), \quad (4)$$

where k is the modal stiffness of the constraint for all of the free cantilever modes and \mathcal{O} denotes the order as $k \rightarrow 0$. Equation (4) shows that the first-order effect of k is to stiffen the modes proportionally without affecting the unconstrained eigenfunctions. On the other hand, if $k \gg \beta_i^-$, then β_i^+ tends to the i th root of the characteristic equation of a clamped-pinned beam. Nevertheless, for all finite k , there exists an i that is sufficiently large so that $k \ll \beta_i^- \approx \beta_i^+$.

2.2 Modal truncation

Given the solution (2) to the eigenvalue problem for (1) in the $+$ and $-$ regions, it is tempting to pursue development of a reduced-order, lumped-parameter model using a truncated eigenvalue expansion in each region separately. For a purely linear problem, we know by the eigenfunction expansion theorem [8] that such a procedure will converge. Here however, there is a subtlety because the overall problem is non-linear, and so one should not expect a purely linear eigenfunction expansion to correctly capture the solution.

To resolve this apparent paradox, suppose the exact solution within each region, written in the form

$$w(s, t) = \sum_{i=1}^{\infty} \psi_i^\pm(s) q_i^\pm(t),$$

is decomposed into a truncated series approximation and a residual error:

$$w^{N\pm}(s, t) = \sum_{i=1}^N \psi_i^\pm(s) q_i^\pm(t), \quad e^{N\pm}(s, t) = \sum_{i=N+1}^{\infty} \psi_i^\pm(s) q_i^\pm(t).$$

Indeed, this was the approach adopted by [10] where the first mode of the cantilever and the clamped-pinned beam were retained in a lumped-parameter, single degree-of-freedom, reduced-order model for the dynamics of a cantilever in the presence of a rigid, one-sided constraint. The orthogonality relations of the modes ensure only that $w^{N+}(s, t)$ is orthogonal to $e^{N+}(s, t)$ and $w^{N-}(s, t)$ orthogonal to $e^{N-}(s, t)$. But this is not the case for $w^{N\pm}(s, t)$ and $e^{N\mp}(s, t)$. Consequently, at each switching event between + and - regions, a portion of the exact solution (the residual) is lost when changing basis from the unconstrained to the constrained eigenfunctions or vice versa. Thus, when crossing from the + region to the -, some of the information in w^{N+} is projected onto w^{N-} when we change basis, and vice versa when crossing from - to +. Hence, if simulating for a long time it is not clear *a priori* that this form of modal truncation will converge as $N \rightarrow \infty$, as errors can accumulate upon repeated crossing of the switching condition. In what follows, we shall refer to the eigenbasis $\{\psi_i^+\}$ as the set of *constrained* cantilever modes and $\{\psi_i^-\}$ as the *unconstrained* cantilever modes. To simplify notation we shall let $\phi_i = (-1)^{(i+1)} \psi_i^-$ where the sign of ϕ_i is chosen conveniently so that $\phi_i(1) = 2$ for all i .

A more tractable approach for modal truncation, for which the study of convergence is more straightforward, is to use a single eigenbasis. That is, a reduced-order model is obtained through a Galerkin decomposition using the unconstrained cantilever eigenfunctions $\{\phi_i(s)\}$ as the trial basis. To do this, it is natural to incorporate the interaction force between the beam and the constraint directly in the PDE (1) as an additional forcing term rather than through the boundary conditions. This can be achieved as follows:

$$\begin{aligned} w_{tt}(s, t) + 2\alpha w_t(s, t) + w_{ssss}(s, t) &= \delta(s-1)h(w(1, t)) + f(s, t) \quad (5) \\ s = 0 : \quad w &= w_s = 0 \\ s = 1 : \quad w_{ss} &= w_{sss} = 0, \end{aligned}$$

where

$$h(d) = \begin{cases} 0, & d \leq d_0 \\ -\frac{k}{4}(d - d_0) & d > d_0 \end{cases}. \quad (6)$$

Now, we make a global decomposition

$$w(s, t) = \sum_{i=1}^{\infty} \phi_i(s) \eta_i(t) \quad (7)$$

where the ϕ_i are unconstrained eigenfunctions which are scaled such that orthogonality relation

$$\int_0^1 \phi_i(s)\phi_j(s)ds = \delta_{ij}$$

is enforced with δ_{ij} being the Kronecker delta function. Substitution of (7) into (5) and taking the inner-product with ϕ_j yields

$$\ddot{\eta}_j(t) + 2\alpha\dot{\eta}_j(t) + k_j\eta_j(t) + \phi_j(1)\frac{k}{4}\sum_{i=1}^{\infty}\phi_i(1)\eta_i(t) = \frac{kd_0}{4}\phi_j(1) + f_j(t), \quad (8)$$

where

$$f_j(t) = \int_0^1 \phi_j(s)f(s,t)ds, \quad \text{and } k_j = (\beta_j^-)^4,$$

and a dot is used to denote differentiation in time. Letting

$$\boldsymbol{\eta}(t) = [\eta_1(t), \eta_2(t), \eta_3(t), \dots, \eta_N(t)]^T \quad \text{and } \boldsymbol{\phi}(s) = [\phi_1(s), \phi_2(s), \phi_3(s), \dots, \phi_N(s)]^T,$$

an N degree of freedom (NDOF) reduced-order model may be expressed as

$$\ddot{\boldsymbol{\eta}}(t) + 2\alpha\dot{\boldsymbol{\eta}}(t) + [K^\pm] \boldsymbol{\eta}(t) = \mathbf{F}^\pm(t), \quad (9)$$

where $\mathbf{F}^-(t) = [f_1(t), f_2(t), f_3(t), \dots, f_N(t)]^T$,

$$\mathbf{F}^+(t) = \mathbf{F}^-(t) + \frac{kd_0}{4}\boldsymbol{\phi}(1), \quad K_{ij}^- = \delta_{ij}k_j, \quad \text{and } K_{ij}^+ = \delta_{ij}k_j + k,$$

The switching surface between the + and - regions is now given by

$$\boldsymbol{\phi}^T(1)\boldsymbol{\eta}(t) = d_0.$$

2.3 Modal convergence

Figure 2 shows how the eigenvalues $\lambda_1, \lambda_2, \dots, \lambda_N$ of the stiffness matrix $[K^+]$ approximate the modal stiffnesses $(\beta_1^+)^4, (\beta_2^+)^4, \dots, (\beta_N^+)^4$ of the original continuum model. Notice how, for each value of N , the highest-order mode diverges from the exact solution as $k \rightarrow \infty$. Recall that each β_i^+ of the exact solution tends to the i th mode of the clamped-pinned beam when $k \gg (\beta_i^+)^3$. In the reduced-order model however, as k becomes large, the highest mode corresponds to in-phase contributions of the unconstrained cantilever modes with eigenvector

$$\mathbf{v}_N = [N^{-1/2}, N^{-1/2}, \dots, N^{-1/2}]$$

and eigenvalue $\lambda_N = kN$. Therefore, if k exceeds $\mathcal{O}(\beta_N^+)^3$, the highest eigenfrequency of the truncated model and the exact eigenfrequency diverge.

This non-convergence between eigenvalues of the truncated model and the BVP in the limit $k \rightarrow \infty$ is in fact an unavoidable consequence of performing Galerkin discretization using the unconstrained eigenmodes, which satisfy natural (force and moment free) boundary conditions at the free end. In the limit that the stiffness of the constraint becomes large compared to that of the highest-order included eigenfunction, the stiffness of the constraint at the free end makes the boundary condition much closer to a geometric (pinned) one. Therefore, the unconstrained cantilever modes do not provide a good approximation to the true dynamics. Nevertheless, for a given constraint stiffness k , choosing N such that $(\beta_N^+)^3 \gg k$ ensures that the modal description of the reduced-order model will accurately capture that of the full continuum BVP. In particular, for fixed k , we have modal convergence as $N \rightarrow \infty$.

3 The impact limit; modal restitution laws

A common approach in modelling the dynamics of a flexible beam with a stiff, one-sided constraint has been to consider the so-called impact limit where the constraint becomes rigid. This approach imposes the classical Newtonian coefficient of restitution (CoR) law at a localized point on the continuous beam given by

$$w_t(s_I, t_{I+}) = -rw_t(s_I, t_{I-}), \quad w(s_I, t_I) = d_0, \quad (10a)$$

$$w_t(s, t_{I+}) = w_t(s, t_{I-}), \quad s \neq s_I, \quad (10b)$$

where $0 < r < 1$ is the coefficient of restitution, $t_{I\pm}$ is the time instantaneously after (+) or before (-) an impact occurs and $s = s_I$ is the location of the impact. In what follows, we shall assume that $s_I = 1$, so that impact occurs at the free end of the beam. Incorporating (10) into a modal model has the general form

$$\dot{\boldsymbol{\eta}}(t_{I+}) = -[R]\dot{\boldsymbol{\eta}}(t_{I-}), \quad (11)$$

where $[R]$ is a modal CoR matrix which allows the modal energy to be redistributed post impact. An NDOF, reduced-order, impact model is established once the modal CoR matrix $[R]$ is determined .

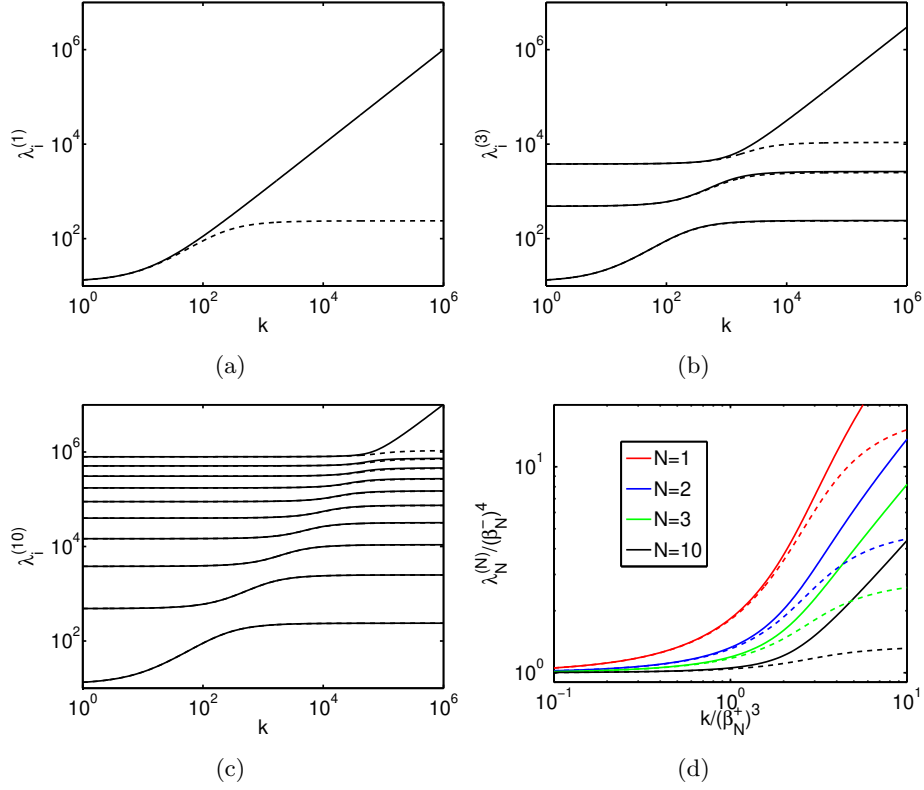


Figure 2: Comparison between the constrained eigenfrequencies of the full BVP (dashed lines) and the constrained eigenfrequencies of the reduced-order model (solid lines) for (a) 1DOF, (b) 3DOF, and (c) 10DOF reduced-order models. (d) Scaled representation of the highest eigenfrequency in (a)-(c).

3.1 Restitution law via collocation

Wagg and Bishop [28] (see also [26]) introduced a straightforward way to determine $[R]$, by enforcing (10) to hold at a set N *collocation* points s_j , $j = 1, 2, \dots, N-1$, along the beam. The modal CoR matrix $[R]_C$ calculated

via such an approach is simply

$$[R]_C = \begin{bmatrix} \phi^T(s_1) \\ \phi^T(s_2) \\ \vdots \\ \phi^T(s_{N-1}) \\ \phi^T(s_I) \end{bmatrix}^{-1} \begin{bmatrix} -1 & 0 & \dots & 0 & 0 \\ 0 & -1 & \dots & 0 & 0 \\ \vdots & \vdots & \ddots & & \ddots \\ 0 & 0 & \dots & -1 & 0 \\ 0 & 0 & \dots & & r \end{bmatrix} \begin{bmatrix} \phi^T(s_1) \\ \phi^T(s_2) \\ \vdots \\ \phi^T(s_{N-1}) \\ \phi^T(s_I) \end{bmatrix}. \quad (12)$$

Note, as pointed out in [25], that $[R]_C$ is non-unique due to the arbitrariness in the choice of the s_i . Nevertheless, if the s_i are chosen to be equally spaced along the beam, then, in the limit as N becomes large, one might expect $[R]_C$ to converge, making this approach somewhat analogous to finite element analysis.

3.2 Impulse-response restitution law

An alternative method for determining the modal CoR, proposed in [25], is to consider the impulse response of the reduced-order model and determine the magnitude of the impulse required to enforce (10)a. To obtain such a matrix, consider a cantilever subjected to an isolated impulsive point force

$$w_{tt}(s, t) + w_{ssss}(s, t) = p_0 \delta(s - s_I) \delta(t), \quad (13)$$

where p_0 is the magnitude of the impulse. Pursuing a solution to (13) via eigenfunction expansion involves writing $w(s, t) = \sum_{i=1}^{\infty} \psi_i^-(s) q_i^-(t)$ and truncating the series after N terms. Choosing $s_I = 1$, projecting the solution onto the j th mode and solving for $q_j^-(t)$ yields

$$q_j^-(t) = p_0 \psi_i^-(1) (\beta_j^-)^{-2} \sin(\beta_j^-)^2 t, \quad t > 0.$$

Substitution of the truncated modal expansion for the impulse response into (10) solves for the unknown p_0 and establishes the relationship

$$\dot{q}_j^-(t_{I+}) = \dot{q}_j^-(t_{I-}) - \frac{r+1}{N} \sum_{i=1}^N \dot{q}_i^-(t_{I-}).$$

Following this approach, the *impulse-response* CoR $[R] = [R]_{IR}$ for the 2DOF, reduced-order model is given by

$$[R]_{IR} = \frac{1}{N} \begin{bmatrix} r+1-N & r+1 & \dots & r+1 \\ r+1 & r+1-N & \dots & r+1 \\ \vdots & \vdots & \ddots & r+1 \\ r+1 & r+1 & r+1 & r+1-N \end{bmatrix} \quad (14)$$

4 Restitution law via infinite stiffness limit

Rather than impose the CoR law in (10) *a priori*, we shall now seek to derive a general form of CoR by considering the modal compliant model in the limit that the constraint stiffness $k \rightarrow \infty$.

To this end, suppose we let $k = \varepsilon^{-2}\kappa$, where $0 < \varepsilon \ll 1$ is a scaling parameter and $\kappa = \mathcal{O}(1)$ as $\varepsilon \rightarrow 0$. In this case it is straightforward to see that the time taken for a trajectory of the dynamical system to pass through the + region is $\mathcal{O}(\varepsilon^{-1})$. Thus, if we take the limit $\varepsilon \rightarrow 0^+$, this time tends to zero and we will have an equivalent impact oscillator with a modal impact law (11). The question arises how the impact law $[R]_N$ derived by this asymptotic approach applied to the compliant N -modal truncation will correspond to either $[R]_C$ or $[R]_{IR}$. The convergence properties of $[R]_N$ as $N \rightarrow \infty$ are also of interest. In order to answer these questions, we shall consider separately the cases $N = 1$ and $N = 2$, before tackling the general case. Finally, to simplify the analysis, we consider the special case of $d_0 = 0$.

4.1 Single-degree-of-freedom impact oscillator

Consider the single degree-of-freedom (1DOF) compliant model with initial conditions on the switching surface and impending motion in the + region:

$$\begin{aligned} \ddot{\eta}_1(t) + 2\alpha\dot{\eta}_1(t) + (k_1 + k)\eta_1(t) &= f_1(t), \quad \eta_1(t) \geq 0, \\ \eta_1(0) &= 0, \quad \dot{\eta}_1(0) = \varepsilon^{-1}v^+ > 0. \end{aligned} \quad (15)$$

Letting $k = \varepsilon^{-2}\kappa$, $t = \varepsilon\tau$ and $\xi = \eta_1$, we can rewrite (15) as

$$\begin{aligned} \xi_{\tau\tau} + 2\alpha\varepsilon\xi_\tau + \kappa\xi &= \mathcal{O}(\varepsilon^2), \quad \xi > 0 \\ \xi(0) &= 0, \quad \xi_\tau(0) = v^+. \end{aligned} \quad (16)$$

Substituting $\xi = \xi^0 + \varepsilon\xi^1 + \dots$ into (16) and collecting terms by order of ε yields

$$\mathcal{O}(\varepsilon^0): \quad \xi_{\tau\tau}^0 + \kappa\xi^0 = 0, \quad \mathcal{O}(\varepsilon^1): \quad \xi_{\tau\tau}^1 + \kappa\xi^1 = -2\alpha\xi_\tau^0,$$

which has solution

$$\xi(\tau) = v^+\kappa^{-1/2}(1 - \varepsilon\alpha\tau)\sin\kappa^{1/2}\tau + \mathcal{O}(\varepsilon^2), \quad 0 \leq \tau \leq \Delta^+, \quad (17)$$

where

$$\Delta^+ = \pi\kappa^{-1/2} \quad (18)$$

is the time of passage in the + region. Differentiating (17) with respect to time and substituting $\tau = \Delta^+$, we find

$$v^- = -r_e v^+, \quad \text{with } r_e = 1 - \alpha\pi\kappa^{-1/2}\varepsilon \quad (19)$$

where v^- is the velocity when the oscillator re-enters the - region. We therefore call r_e the *effective* coefficient of restitution.

Figure 3(a) shows a comparison between the return velocity v^- predicted by the impact law (19) and that obtained by simulating the 1DOF model (15) for different values of the constraint stiffness. Specifically, letting $k = \varepsilon^{-2}$, $\eta_1(0) = 0$ and $\dot{\eta}_1(0) = \varepsilon^{-1}$, the effective restitution coefficient r_e^2 is compared to the computed $(v^-/v^+)^2$, as ε is varied. Note from the figure, the close agreement for small ε . Also, note $r_e \rightarrow 1$ in the limit as $\varepsilon \rightarrow 0^+$. However, in experiments, Thompson et al [23] observed low values of the coefficient of restitution that were attributed to energy transfer to higher modes during contact. Hence, we will next consider the impact limit of the 2DOF model.

4.2 Two degrees of freedom

Next, we consider the effect of an additional mode. For a 2DOF reduced-order model to the + region, the governing equation reduces to

$$\ddot{\boldsymbol{\eta}}(t) + 2\alpha\dot{\boldsymbol{\eta}}(t) + [K^+] \boldsymbol{\eta}(t) = \mathbf{F}^-(t), \quad \boldsymbol{\phi}^T(1)\boldsymbol{\eta}(t) > 0. \quad (20)$$

Substituting $k = \kappa\varepsilon^{-2}/2$ into $[K^+]$ and scaling by ε^2 , we find the eigenvectors are

$$[V] = \frac{1}{\sqrt{2}} \begin{bmatrix} 1 & 1 \\ -1 & 1 \end{bmatrix} + \mathcal{O}(\varepsilon^2). \quad (21)$$

Letting $\boldsymbol{\eta}(t) = [V] \mathbf{q}(t)$, $\mathbf{q}(t) = [q_1(t), q_2(t)]^T$ and $t = \varepsilon\tau$, (20) can be expressed as

$$\mathbf{q}_{\tau\tau}(\tau) + 2\alpha\varepsilon\mathbf{q}_\tau(\tau) + \begin{bmatrix} 0 & 0 \\ 0 & \kappa \end{bmatrix} \mathbf{q}(\tau) = \mathcal{O}(\varepsilon^2), \quad q_2(\tau) > 0. \quad (22)$$

Notice that q_1 is orthogonal to the switching surface. The lowest-order mode imitates a clamped-pinned beam mode with zero amplitude at the free end. Letting $\xi = q_2$ we recover (16) for the 1DOF oscillator. It follows that the velocity of q_2 obeys the impact law given in (19). Additionally, integrating the equation for q_1 and expanding in powers of ε , we relate $q_{1\tau}(0) = v_1^+$ to the return velocity $q_{1\tau}(\Delta^+) = v_1^-$ by

$$v_1^- = v_1^+ \left(1 - 2\alpha\pi\kappa^{-1/2}\varepsilon \right) + \mathcal{O}(\varepsilon^2). \quad (23)$$

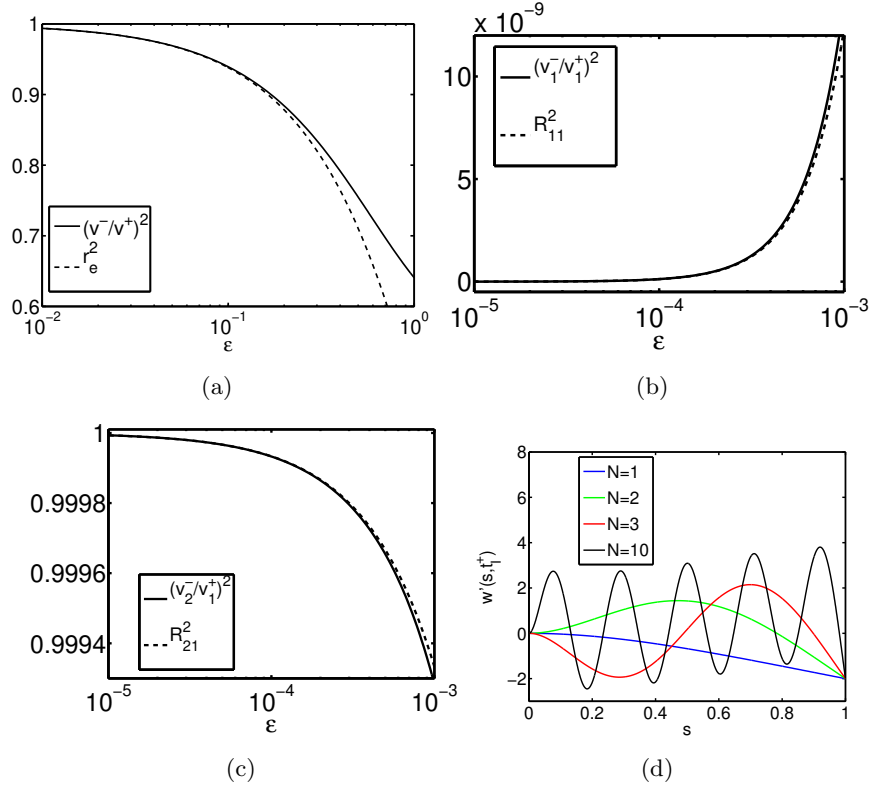


Figure 3: (a)–(c) Comparison between the impact law derived from a perturbation approach (dashed line) and numerical simulations using an NDOF reduced-order compliant model (solid line) with $F = 0$, $\alpha = 0.1$, $k = \epsilon^{-2}$ and $v^+ = \epsilon^{-1}$ in the first mode: (a) $N = 1$; and (b,c) $N = 2$, showing first and second mode respectively. (d) Post-impact velocity profile $w_t^N(s, t_t^+)$ predicted by the NDOF impact law for $\mathbf{v}^- = [1, 0, 0, \dots, 0]^T$.

Thus, the modal coefficient of restitution is given by

$$[R]_2 = [V] \begin{bmatrix} 1 - 2r_e & 0 \\ 0 & r_e \end{bmatrix} [V]^T. \quad (24)$$

Substituting $[V]$ from (21) into (24) we find

$$[R]_2 = \frac{1}{2} \begin{bmatrix} r_e - 1 & 1 - 3r_e \\ 1 - 3r_e & r_e - 1 \end{bmatrix}. \quad (25)$$

Notice that $[R]_2$ deviates in the off-diagonal terms from the expression (14) for the impulse-response restitution law $[R]_{IR}$. The source of the discrepancy is that the energy loss captured in r_e is from the external viscous damping, whereas r in (14) captures the *ad-hoc* energy dissipation modelled by the Newtonian impact law. We note that both converge in the limit as r and r_e tend to unity.

The dynamics of the 1DOF and 2DOF impact models are fundamentally different post impact. To see this, consider pre-impact, initial conditions

$$\boldsymbol{\eta}(0) = \mathbf{0}, \quad \text{and } \dot{\boldsymbol{\eta}}(t) = \mathbf{v}^+ = [\varepsilon^{-1}v_1^+, 0]^T.$$

The oscillator returns to the $-$ region with a velocity

$$\mathbf{v}^- = \varepsilon^{-1} [v_1^-, v_2^-]^T, \quad \text{where } v_1^- = -R_{11}v_1^+, \quad v_2^- = -R_{21}v_1^+,$$

and R_{11} and R_{21} are the elements from $[R]_2$. Letting $k = \varepsilon^{-2}$, the post-impact velocities predicted by the impact law are compared to numerical simulations of the reduced-order, compliant model as ε is varied in Fig. 3(b,c). In the case of the 2DOF model, the effective coefficient of restitution of the first mode tends to zero as $\varepsilon \rightarrow 0^+$. In other words, the motion of the first mode of the 2DOF reduced-order model in the impact limit becomes completely uncorrelated with the motion of the equivalent 1DOF model after the first impact.

4.3 General N degree-of-freedom case

For the N degree-of-freedom case, let $\kappa = kN\varepsilon^2$. Following the approach for the 2DOF case, we substitute $\mathbf{q}(t) = [V]^T \boldsymbol{\eta}(t)$ to diagonalize (9) in the $+$ region. Without solving for either $[V]$ or $[\Lambda]$, we know that $\lambda_j = \mathcal{O}(\varepsilon^2)$ for $j < N$ and $\lambda_N = \kappa + \mathcal{O}(\varepsilon^2)$ and the eigenvectors are mutually orthogonal with the eigenvector of the high-frequency mode given by

$$\mathbf{v}_N = [N^{-1/2}, N^{-1/2}, \dots, N^{-1/2}]^T. \quad (26)$$

It follows that the equation of motion in the + region can be expressed as

$$\mathbf{q}_{\tau\tau}(\tau) + 2\alpha\varepsilon\mathbf{q}_\tau(\tau) + \begin{bmatrix} 0 & 0 & \dots & 0 \\ 0 & 0 & \dots & 0 \\ \vdots & \vdots & \ddots & 0 \\ 0 & 0 & 0 & \kappa \end{bmatrix} \mathbf{q}(\tau) = \mathcal{O}(\varepsilon^2), \quad q_N(\tau) > 0. \quad (27)$$

Substituting $\xi = q_N$ into the equation for the N th mode in (27), we again recover (16). Accordingly, the time of passage in the + region and the return velocity of the N th mode are again given by (18) and (19), respectively. The equations for q_j , $j < N$ are again over-damped oscillators for which the return velocities are predicted by (23). It follows that the NDOF modal coefficient of restitution is given by

$$[R]_N = [V] \begin{bmatrix} 1 - 2r_e & 0 & \dots & 0 \\ 0 & 1 - 2r_e & \dots & 0 \\ \vdots & \vdots & \ddots & 0 \\ 0 & 0 & 0 & r_e \end{bmatrix} [V]^T. \quad (28)$$

From (26) and given that $[V]$ is an orthogonal matrix, it is possible to show

$$[R]_N = \begin{bmatrix} 1 - 2r_e + \frac{3r_e - 1}{N} & \frac{3r_e - 1}{N} & \dots & \frac{3r_e - 1}{N} \\ \frac{3r_e - 1}{N} & 1 - 2r_e + \frac{3r_e - 1}{N} & \dots & \frac{3r_e - 1}{N} \\ \vdots & \vdots & \ddots & \frac{3r_e - 1}{N} \\ \frac{3r_e - 1}{N} & \frac{3r_e - 1}{N} & \frac{3r_e - 1}{N} & 1 - 2r_e + \frac{3r_e - 1}{N} \end{bmatrix} \quad (29)$$

Substituting $N = 1$ and $N = 2$ recovers the results for the 1DOF and 2DOF oscillators, respectively.

4.4 Modal non-convergence as $N \rightarrow \infty$

Modal non-convergence in the impact limit can be demonstrated readily with the NDOF modal CoR given in (29). The post-impact velocity profile is given by

$$w_t^N(s, t_{I+}) = -\phi^T(s) [R]_N \mathbf{v}^-. \quad (30)$$

For the truncated model to converge, $w_t^N(s, t_I^+)$ must converge for a given \mathbf{v}^- as $N \rightarrow \infty$. However, increasing N in the $[R]_N$ excites higher-order modes to the same degree as the lower-order modes.

Fig. 3(d) shows the truncated approximation for the post-impact velocity distribution $w_t^N(s, 0^+)$ for $N = 1, 2, 3, 10$, $r_e = 1$ and $\mathbf{v}^- = [1, 0, 0, \dots, 0]^T$.

Clearly, the post-impact velocity does not converge as modes are added to the restitution law. This non-convergence comes from taking an N -modal model, passing to the impact limit $\varepsilon \rightarrow 0$, and then considering what happens as $N \rightarrow \infty$. It would appear that these two separate limiting processes are incommensurate.

To gain further insight, it is instructive to consider again the results in Fig. 2. This shows that modal convergence in the impact limit is achieved only if the limits $\varepsilon \sim k^{-1/2} \rightarrow 0$ and $N \rightarrow \infty$ are taken together. That is, for each N there is a maximum value of $k = \mathcal{O}(\beta_N^+)^3$ for which the model gives answers that are commensurate with other modal truncations. However, modelling the interaction with the constraint with an impact law also requires $k \gg \mathcal{O}(\beta_N^+)^4$. At least for a uniform cantilever beam, the two conditions are incompatible. Thus to accurately model the interaction between the cantilever and the constraint in a truncated model requires a compliant formulation.

5 Numerical studies

In the previous section we found that for the eigenfrequencies of the reduced-order model to converge to the exact solution of the continuous BVP required $k \ll \mathcal{O}(\beta_N^+)^3$. However, since the system is non-linear, this requirement is only a necessary condition for convergence. As k becomes large the excursion of the oscillator into the $+$ region is characterised by increasingly small length scales where contributions from higher-order modes may not be considered negligible. To study convergence of the non-linear system we turn to numerical simulations. Numerical simulations using the model studied so far led to qualitatively similar results to those presented in what follows (although there was a quantitative difference in the amount of damping seen in the higher modes). However, to get an acceptable match with experimental results presented in the next Section, we found it necessary to include material damping in addition to the viscous damping from the surrounding fluid.

5.1 Inclusion of material damping

The simplifying assumption in the previous sections of linear, mass-proportional damping enabled two sets of uncoupled modes corresponding to the $+$ and $-$ regions, which made the analysis tractable. If we now add material damping

to (5) we have

$$w_{tt}(s, t) + 2\alpha w_t(s, t) + \gamma w_{ssst}(s, t) + w_{ssss}(s, t) = \delta(s - 1)h(w(1, t)) + f(s, t) \quad (31)$$

$$s = 0: \quad w = w_s = 0 \quad (32)$$

$$s = 1: \quad w_{ss} = w_{sss} = 0 \quad (33)$$

where γ is the coefficient of stiffness-proportional material damping, and $h(\cdot)$ is given (6). Again, using a trial basis $\phi_i(s)$ corresponding to the normal modes of the simple cantilever, the NDOF Galerkin model becomes

$$\ddot{\boldsymbol{\eta}}(t) + [C] \dot{\boldsymbol{\eta}}(t) + [K^\pm] \boldsymbol{\eta}(t) = \mathbf{F}^\pm(t), \quad (34)$$

where $C_{ij} = (2\alpha + \gamma k_j)\delta_{ij}$ is the modal damping attenuation and K^\pm and \mathbf{F}^\pm have the same meaning as in (9).

While in the $-$ region, the damping operator can be written as a linear combination of the mass and stiffness operators. However, in the $+$ region, we find full coupling, which renders the perturbation analysis in the previous section less tractable. Nevertheless we should expect similar conclusions.

On the other hand, (9) and (34) are equally amenable to numerical analysis. Representing (34) in state-space form

$$\dot{\mathbf{x}} = [A^\pm] \mathbf{x} + \hat{\mathbf{F}}^\pm(t) \quad (35)$$

where

$$\mathbf{x}(t) = \begin{bmatrix} \boldsymbol{\eta}(t) \\ \dot{\boldsymbol{\eta}}(t) \end{bmatrix}, [A^\pm] = \begin{bmatrix} [0] & [I] \\ -[K^\pm] & -[C] \end{bmatrix}, \hat{\mathbf{F}}^\pm(t) = \begin{bmatrix} \mathbf{0} \\ \mathbf{F}^\pm(t) \end{bmatrix}$$

The solution of (35) is

$$\mathbf{x}^\pm(t) = \exp \{ [A^\pm](t - t_0) \} \mathbf{x}_0^\pm + \int_{t_0}^t \exp \{ [A^\pm](t - t') \} \hat{\mathbf{F}}^\pm(t') dt', \quad (36)$$

where $\mathbf{x}_0^\pm = \mathbf{x}_0(t_0)$ is an initial condition either on the switching surface or, or in the case that $f(t)$ is periodic with period ω , on the stroboscopic Poincaré section $\{\omega t = 0 \bmod 2\pi\}$. In the latter case, t_0 can be reset to 0 without loss of generality. Note that the convolution integral in (36) can be evaluated by parts.

5.2 Simulation via root finding

The difficulty in using the explicit solution (36) for simulation arises when solving for the times-of-passage Δ^\pm in the $+$ and $-$ region, which are the roots of a transcendental equation. These can be found using a numerical root-finding algorithm. To ensure that near-grazing events with the switching surface are detected, a golden-section search method is used to identify local extrema in the trajectory of $d(t)$ on the bounded interval from $[t_0, 2\pi/\omega]$. The trajectory is then segmented such that $d(t)$ is monotonic on each segment with at most one root. The bisection method is used to find the root of the first segment to cross the switching surface.

For the numerical simulations we choose the parameters $d_0 = 0$, $\alpha = 0$ and define $\zeta_1 = \gamma (\beta_1^-)^{-2} / 2 = 0.01$, which is the damping ratio of the fundamental mode. Additionally, we choose the specific form of harmonic forcing given by

$$f(x, t) = \frac{k_1 \psi_1(s)}{2\zeta_1 \psi_1(1)} \cos \omega t, \quad \text{with } \omega = 2 (\beta_1^-)^2, \quad (37)$$

which projects purely to the first mode, and has frequency set to the effective resonance of the fundamental mode in the impact limit [18]. The amplitude of $f(x, t)$ is chosen, without loss of generality, so that the unconstrained amplitude of $w(1, t)$ is unity when $\omega = (\beta_1^-)^2$.

To simulate periodic orbits, we choose initial conditions $\mathbf{x}^+(0) = 0$ and discard the first 1000 excitation cycles. We then say that the resulting trajectory is a period- m orbit if $\|\mathbf{x}(t_0 + 2\pi m/\omega) - \mathbf{x}(t_0)\| < 1 \times 10^{-9}$. Such a periodic orbit with n impacts is denoted (m, n) .

5.3 Results

Figure 4 compares numerically simulated periodic orbits for the truncated, bilinear model with $N = 1, 2, 3, 10$ and $k = 100k_1 = \mathcal{O}(k_2)$. In each case, the above numerical procedure resulted in a unique periodic orbit. For the 1DOF model, this is a simple $(1, 1)$ -orbit. However, for the 2-, 3- and 10DOF models there are additional complexities due to the higher-order modes contributing significantly to the interaction between the cantilever and the constraint. Thus, the 2DOF model predicts a $(2, 4)$ orbit, whereas the 3DOF-model has converged to a $(1, 3)$ -orbit. Essentially the first impact excites high frequency modes which result in additional taps on the constraining surface. In contrast the 10DOF model converges to a $(1, 1)$ orbit with a complex interaction with the constraint. While m and n are equal

for the 10DOF and 1DOF case, quantitatively the 10DOF model is closer to the 3DOF model. The additional modes in the 10DOF model provide a mechanism for rapid energy dissipation during the interaction since the modal damping attenuation goes as $(\beta_i^-)^2$ for the material damping model.

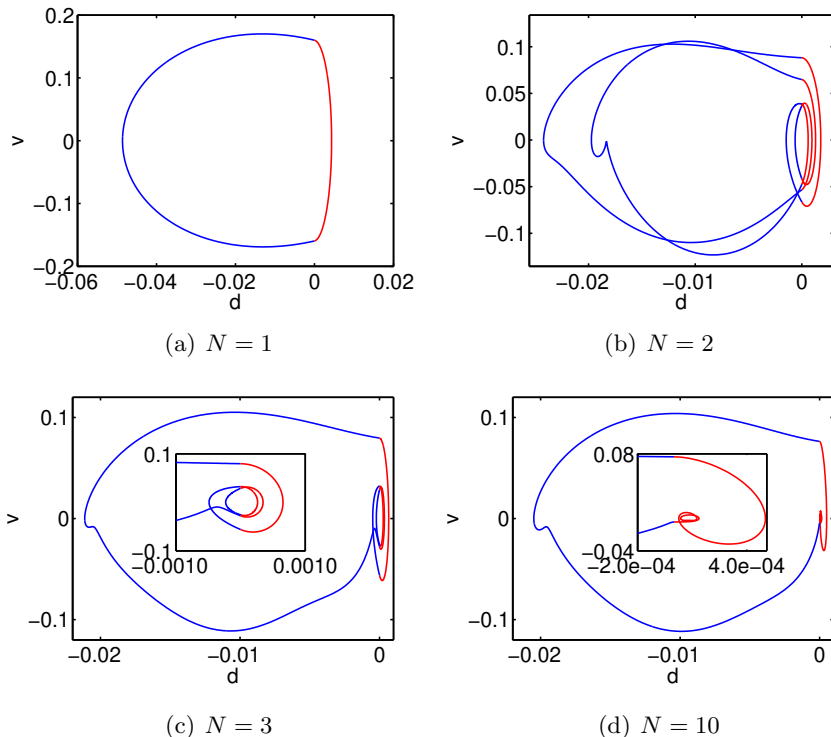


Figure 4: Simulated periodic orbits of the NDOF, bilinear oscillator (34) for $N = 1, 2, 3, 10$ in panels (a)–(d) respectively. Segments of the orbit in blue correspond to the $-$ region and segments in red to the $+$ region. Parameter values chosen are $k = 100k_1$, $\alpha = 0$, $\gamma = 0.02 (\beta_1^-)^2$, and the forcing function is given by (37).

We now compare what happens to the corresponding bifurcation diagrams as we vary the constraint stiffness k , with the other parameters held at $\zeta_1 = 0.01$, $d_0 = 0$, $\alpha = 0$ and $\omega = 2(\beta_1^-)^2$. Fig 5 shows results of the computation of a “brute-force” bifurcation diagram depicted in the impact ($d = d_0$, $v > 0$) Poincaré section.

Note that for small k ($k \leq \mathcal{O}(k_1)$) each model predicts a stable $(1, 1)$

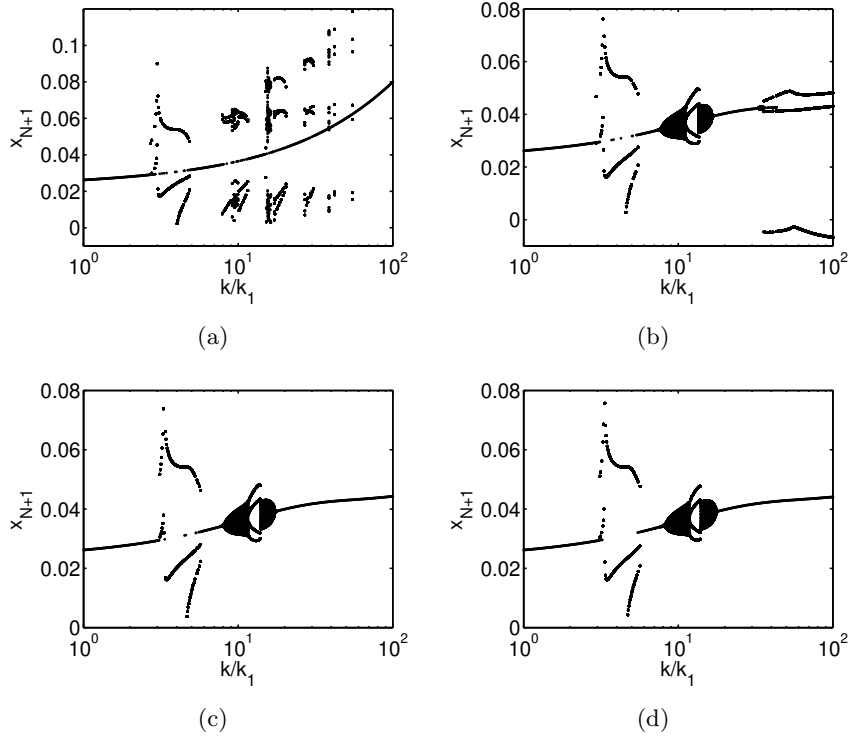


Figure 5: Monte Carlo bifurcation diagrams for NDOF truncated models with $N = 1, 2, 3, 10$ in panels (a)–(d) respectively, as k varies. All other parameters held as in Fig. 4.

periodic orbit with quantitative agreement. As k approaches $\mathcal{O}(k_2)$ ($k_2 \approx 39.3k_1$), higher-order modes couple into the response during interaction with the constraint. These modes couple into the response much more rapidly than study of the linear convergence in §2 would suggest. That is, although the lowest order modes have converged reasonably well for $k \gtrsim \mathcal{O}(k_2)$, the relatively-high stiffness of the constraint allows small contributions from higher-order modes to significantly affect the overall interaction between the cantilever and the constraint.

Despite these considerations we can see from the results that $N = 3$ is sufficient to capture the qualitative features of the bifurcation although, as we shall see, this is not universally true throughout the range of parameter values.

5.4 Effective energetic coefficient of restitution via simulation

When conducting numerical simulations, one possible approach for deriving an equivalent impact model of low degree of freedom is to compute an effective CoR by estimating the energy lost to higher-order modes through impact. We shall consider just such an approach to define a so-called *energetic coefficient of restitution* r_E which captures such energy lost from the fundamental mode in a 1DOF impact model — see [21, 27] and references therein for related approaches in the literature.

Equating the energy lost during impact of a 1DOF impact oscillator to the energy lost from the fundamental mode of the NDOF bilinear oscillator in a single impact leads to an implicit definition of r_E for that impact:

$$\frac{1}{2} (1 - \tilde{r}_E^2) (v_1^+)^2 + \int_{t_i}^{t_i+\Delta} F_c[d(t')] \dot{\eta}_1(t') dt' = 0. \quad (38)$$

Here $t = t_i$ is the time instant at which passage occurs from the $-$ region to the $+$ region in the NDOF system, at which time the first mode has velocity v_1^+ , Δ is the time of passage in the $+$ region, η_j is j th modal coordinate of the NDOF bilinear oscillator and

$$F_c(d) = \begin{cases} 0 & d \leq d_0 \\ \frac{k}{4}(d_0 - d)\phi_1(1), & d > d_0, \end{cases}$$

is the interaction force between the beam and the constraint.

We can then define a single energetic coefficient r_E for a specific set of parameters and initial conditions, assuming repeated impacts occur via:

$$\frac{1}{2} (1 - r_E^2) \sum_{i=1}^{\infty} (v_1^{+(i)})^2 + \lim_{t \rightarrow \infty} \int_{t_0}^t F_c[d(t')] \dot{\eta}_1(t') dt' = 0, \quad (39)$$

where t_i and $v_1^{+(i)}$ are the set of impact times and corresponding velocities.

Note that there can be numerical difficulties in evaluation of (39). In the case that motion converges to a periodic orbit, the limit can be evaluated simply by taking t_0 to be a time after a transient behaviour has decayed, and evaluating the integral and sum over a single period. But, for an arbitrary set of parameters, there is no guarantee that the limit in (39) will converge, nor that the limit will be unique over different initial conditions. For instance, it is known that even 1DOF impact oscillators can undergo chattering sequences, in which there are an infinite number of impacts in

a finite time, and can feature coexisting attractors for the same parameter values — see [4] and references therein.

Figure 6 shows a comparison between the dynamics of 20DOF bilinear oscillator and the 1DOF impact oscillator with energetic coefficient of restitution computed using the above approach. In both cases, the motion converges to a periodic orbit, and there is therefore a unique, computable, solution to (39).

In the case depicted in Fig. 6(a), $d_0 = 0.8$, there is relatively large damping and parameters are chosen so that all initial conditions converge to a $(1, 1)$ orbit that is close to grazing. In this case, the computation (39) predicts $r_E = 0.036$ and there is a good quantitative agreement between the 20DOF model and the effective 1DOF impact oscillator. In this case, only a small portion of the total energy stored in the oscillator is redistributed to higher modes during impact which is subsequently dissipated as the damping is sufficiently high. Nevertheless, $r_E = 0.036$ is significantly lower than that which would be predicted from a naive single-degree-of-freedom model using a typical value of 0.5–0.8 for the CoR for macroscopic collisions of steel on steel.

The case depicted in Fig. 6(b) is more like that in Fig. 4, in which $d_0 = 0$, and the damping is relatively weak. Here, (39) predicts $r_E = 0.74$, which is closer to what one would expect from macroscopic impact theory. However, the results show that there is neither good quantitative nor qualitative agreement between the 1DOF impact model and the 20DOF bilinear model. Two particular effects that are due to the higher-order modes are the ‘multiple-tap’ dynamics of the impact where there are two separate intervals in the $-$ region, and the large additional oscillations in the dynamics which are not damped out during the free motion away from the stop.

6 Experiments

In this section we present the results obtained from the experimental rig depicted in Fig. 7. A mild steel cantilever beam with dimensions 300 mm \times 25.5 mm \times 1 mm was mounted on a shaker table. A pin constraint was also mounted on a second cantilever beam with dimensions 300 mm \times 25.5 mm \times 12 mm. From the dimensions of the cantilever and the constraint, we estimate $k/k_1 = \mathcal{O}(10^3)$. The natural frequency $\omega_1 = 2\pi \times 5.92$ rad/s and damping ratio $\zeta_1 = 7.7 \times 10^{-4}$ of the fundamental mode was determined from a ring-down test. Velocity measurements at the point on the beam

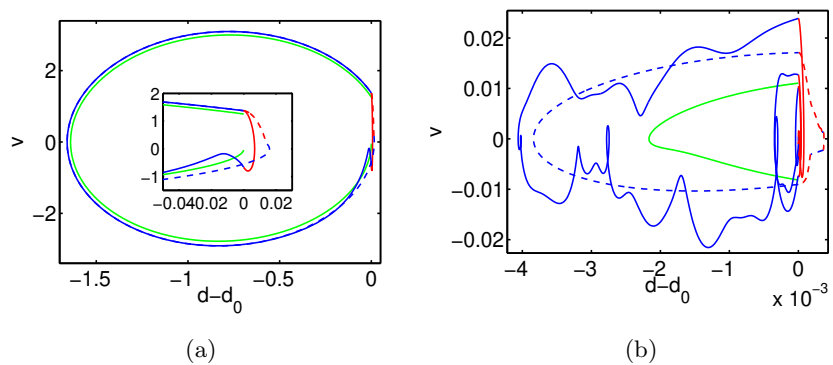


Figure 6: Comparison between the 20DOF bilinear model for $k = 1000k_1$ and the 1DOF impact model. The solid and dashed lines in blue and red correspond to the motion of the free-end and the component from the first mode of the 20DOF bilinear model. The 1DOF impact model is shown in green. (a) (1, 1) orbits near grazing with $d_0 = 0.8$, $\omega = 1.15(\beta_1^-)^2$ and $\zeta_1 = 0.1$. $k = 1000k_1$ for the bilinear oscillator and $r_E = 0.036$ for the impact oscillator. (b) Periodic orbits for $d_0 = 0$, $\omega = 2(\beta_1^-)^2$ and $\zeta_1 = 0.01$ and $r_E = 0.74$.

corresponding to the location of the constraint was made with a Polytec OFV-5000 laser Doppler vibrometer (LDV) in the ground frame. However, due to the low damping, the motion of the base is much smaller than the free-end of the beam and can be neglected. The velocity signal from the LDV is sampled at 50 kHz and has a resolution of $4 \mu\text{m/s}$.

In addition to the velocity measurement, a simple electronic circuit was used to accurately determine when the stop and the beam are in contact. The circuit consists of two resistors in series which are supplied with a constant voltage V_0 . The cantilever beam and constraint act as a switch that shorts the first resistor when the beam is in contact with the constraint. The voltage over the second resistor was sampled at 100 kHz.

To excite the cantilever the shaker table is used to prescribe a harmonic motion to its base. The motion of the base imparts a uniformly distributed inertial force on the cantilever. The inertial force projects onto each eigenmode, however, the effect on higher eigenmodes is minimal because (i) the excitation frequency is closest to the fundamental mode and (ii) the higher modes are substantially stiffer than the fundamental. Consequently, the forcing from the base excitation of the physical system can be approximated by (37).

Figure 8(a) shows the results of a particular experimental run over one period $T = 2\pi/\omega$ of the forcing, obtained after transients had been allowed to decay. The motion was found to be approximately periodic, and the presented results are typical of what happens on each period. Approximately, when viewed at a macro scale, this is a (1,1) periodic orbit. However, the detailed time series (shown in two successive zooms in Fig. 8(b,c)) reveal the motion actually to be more highly structured and to contain five separate time intervals in which the beam is in contact with the stop. There is also evidence of high-frequency, undamped motion between each of the impacts. It would be tempting to wonder if the high-frequency motion is due to measurement noise. However, a comparison between the excited motion of the beam without the stop in Fig. 8(d) reveals that the high-frequency response is several orders of magnitude above the noise threshold.

Figure 9 shows simulation results for the 20DOF bilinear model at the same parameters values as those estimated from the experimental data. Note the strong qualitative similarity with the experimental data; that there is similar multiple-tap dynamics with five separate impacts, and significant energy in the higher modes.

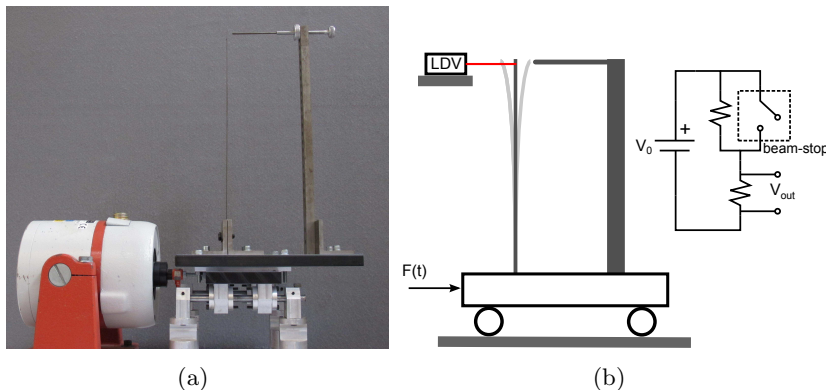


Figure 7: (a) Impacting beam experimental set-up consisting of a flexible cantilever beam and constraint mounted on a shaker table. (b) A schematic of the impacting beam and measurement system. The velocity at the point of impact, which is near to the free-end, is measured by a LDV mounted in the ground frame. A simple circuit is used to determine precisely when the beam is in contact with the constraint.

7 Discussion

The key result of this paper has been to show that the two limiting processes of taking an infinite stiffness limit and an infinite number of modes are incommensurate. That is, one gets a different answer for reduced-order rigid models depending on whether mode truncation or the rigid impact limit is performed first. In fact, as we argued in Section 2, it was already known that there is non-uniqueness of impact laws consistent with Newtonian restitution if one takes modal truncations of a rigid model. (The situation is even worse if one includes friction in the impact — see e.g. [7, 12] and references therein.) We have shown though that the process of taking a succession of modal truncations and passing to the rigid limit separately does not converge. Rather like a Gibbs phenomenon, the residual is never small. This observation is important because, we have found in the simulations that the dynamics observed depends strongly on the number of modes taken in the truncation, with multi-modal models having the propensity to undergo drum-roll-like multiple-tap dynamics with a high-velocity impact followed by several low-velocity impacts in quick succession. The experimental results have shown that this latter form of dynamics occurs in reality.

Moreover, we have shown that attempts to define effective (energetic)

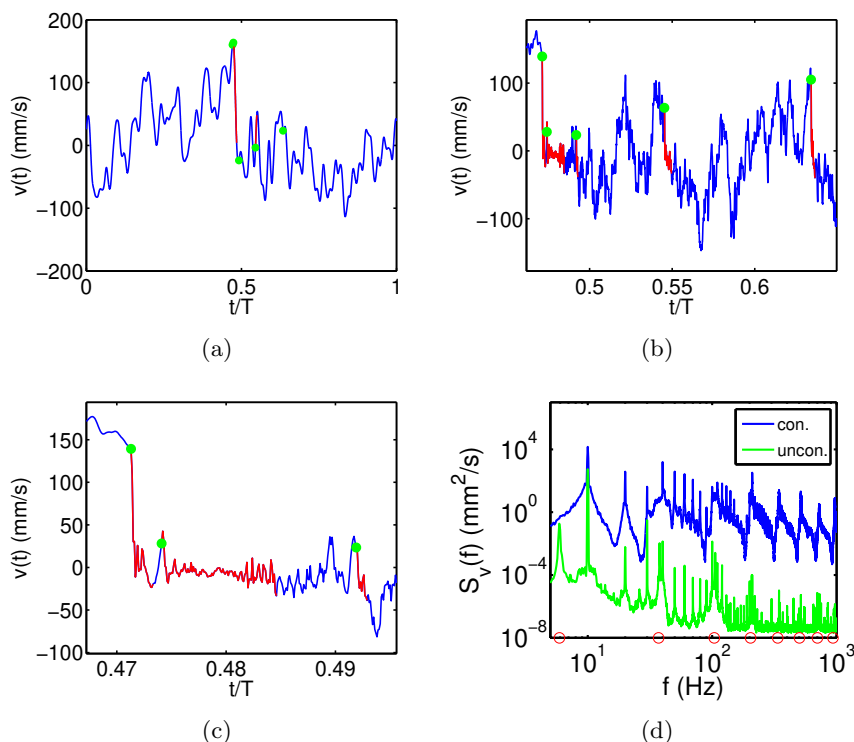


Figure 8: Experimental data obtained from the impacting cantilever. (a) Velocity of signal near to the free-end and (b),(c) two successive zooms. Note that the data in (a) is passed through a low-pass filter for ease of depiction. The blue portion of the time-series represents unconstrained motion, whereas red corresponds to motion in contact; green dots represent time instants at which contact first occurs. (d) The power spectrum S_V corresponding to this motion (blue line), compared with the equivalent results in which the stop is not present. The theoretical unconstrained eigenfrequencies are marked on the x -axis.

restitution laws calculated by estimating the energy transferred to higher-order modes are at best fraught with difficulty, leading to coefficients of restitution that are dependent on the dynamics observed, and can be wildly different from that derivable from a macroscopic consideration. Moreover, in many dynamical regimes, especially where much energy is lost in impact and with low damping, this approach is woefully inaccurate.

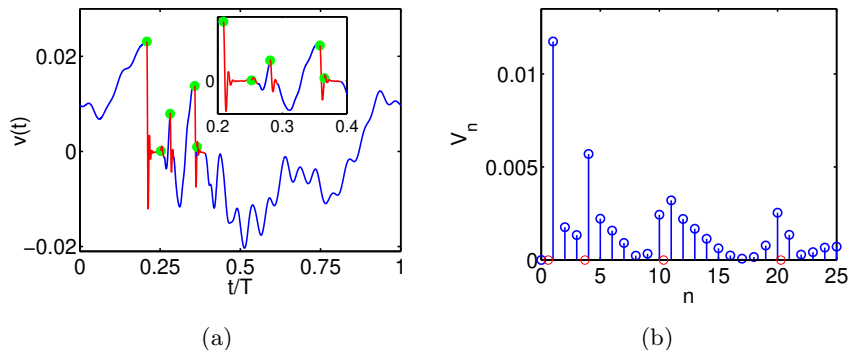


Figure 9: Simulation of the 20DOF, truncated, bilinear model with $\zeta_1 = \gamma(\beta_1^-)^2/2 = 7.7 \times 10^{-4}$, $\alpha = 0$, $\omega = 1.7(\beta_1^-)^2$ and $k = 10^3 k_1$. (a) Velocity waveform for single period. (b) Amplitude spectrum V_n for the first 25 harmonics of the excitation frequency revealing contributions for the first four modes. The unconstrained eigenfrequencies are marked on the x-axis.

The overall conclusion from this paper then is that passing to a rigid limit for a point contact is a dangerous thing to do. It is better to ascribe a large but finite stiffness to the constraint and then to take sufficiently many modes to resolve timescales up to and beyond the timescale of an individual contact.

The present results also have important implications to dynamic AFM, which aims to extract material property information from a sample substrate through the measured response of a microcantilever probe. In this respect, if the probe were to behave as a 1DOF oscillator, the impact limit would represent a singular point at which all material properties of the sample collapse into a single parameter, the coefficient of restitution. Thus, in this limit, quantitative measurements of material properties, such as stiffness/elasticity, viscosity, etc., are not possible. However, the results in this paper show that for an impacting cantilever beam, this limit is never reached since additional modes couple into the dynamics as the stiffness of the constraint is increased. This introduces the possibility of quantitative material property measurements over large variations in sample properties by measuring the response of higher-order modes of the microcantilever.

Acknowledgements

The authors acknowledge useful conversations with Arvind Raman, Oliver Payton and Chris Budd. The work of JM has been sponsored by the UK Engineering and Physical Sciences Research Council.

References

- [1] V.I. Babitskii. *Theory of Vibroimpact Systems. Approximate methods.* Nauka, Moscow, 1978.
- [2] B. Brogliato. *Impacts in Mechanical Systems – Analysis and Modelling.* Springer–Verlag, New York, 2000. Lecture Notes in Physics, Volume 551.
- [3] D.R.J. Chillingworth. Discontinuity geometry for an impact oscillator. *Dynamical Syst.*, 17:380–420, 2002.
- [4] M. di Bernardo, C.J. Budd, A.R. Champneys, and P. Kowalczyk. *Piecewise-smooth dynamical systems; theory and applications.* Springer, New York, 2008.
- [5] J. Emans, M. Wiercigroch, and A.M. Krivtsov. Cumulative effect of structural nonlinearities: chaotic dynamics of cantilever beam system with impacts. *Chaos Soliton. Frac.*, 23(5):1661–1670, March 2005.
- [6] M.I. Feigin. *Forced oscillations in systems with discontinuous nonlinearities.* Nauka, Moscow, 1994. [In Russian].
- [7] D.B. Marghitu and Y. Hurmuzlu. Nonlinear dynamics of an elastic rod with frictional impact. *Mech. Eng.*, 10:187–201, 1996.
- [8] L. Meirovitch. *Principles and Techniques of Vibrations.* Prentice Hall, New Jersey, 1997.
- [9] J. Melcher, X. Xu, and A. Raman. Multiple impact regimes in liquid environment dynamic atomic force microscopy. *Appl. Phys. Lett.*, 93:Art. No. 093111, 2008.
- [10] F.C. Moon and S.W. Shaw. Chaotic vibrations of a beam with nonlinear boundary conditions. *Int. J. Nonlin. Mech.*, 18(v), 1983.
- [11] A. Nordmark. *Grazing conditions and chaos in impacting systems.* PhD thesis, Royal Institute of Technology, Stockholm, Sweden, 1992.

- [12] A. Nordmark, H. Dankowicz, and A. Champneys. Friction-induced reverse chatter in rigid-body mechanisms with impacts. *IMA J. Appl. Math.*, 76:85–119, 2011.
- [13] M. Oestreich, N. Hinrichs, K. Popp, and C.J. Budd. Analytical and experimental investigation of an impact oscillator. *Proc. ASME 16th Biennial Conf. Mech. Vib. Noise*, DETC97VIB-3907:1–11, 1997.
- [14] O. Payton, A.R. Champneys, M.E. Homer, and M.J. Myles. Feedback-induced instability in tapping mode atomic force microscopy: theory and experiment. *Proc. Roy. Soc. A*, 467:1801–1822, 2011.
- [15] F. Peterka. Theoretical analysis of n -multiple $(1/n)$ -impact solutions. *Acta Tech. CSAV*, 26(2):462–473, 1974.
- [16] P.T. Piiroinen, L.N. Virgin, and A.R. Champneys. Chaos and period-adding; experimental and numerical verification of the grazing bifurcation. *J. Nonlin. Sci.*, 14:383–404, 2004.
- [17] A. Raman, J. Melcher, and R. Tung. Cantilever dynamics in atomic force microscopy. *Nano Today*, 3:20–27, 2008.
- [18] S.W. Shaw and P.J. Holmes. A periodically forced piecewise linear oscillator. *J. Sound Vib.*, 90:129–155, 1983.
- [19] S.W. Shaw and P.J. Holmes. Periodically forced linear oscillator with impacts: Chaos and long-period motions. *Phys. Rev. Lett.*, 51:623–626, 1983.
- [20] R.W. Stark. Bistability, higher harmonics, and chaos in afm. *Mater. Today*, 13:24–32, 2010.
- [21] W.J. Stronge. *Impact Mechanics*. Cambridge University Press, 2000.
- [22] J.M.T. Thompson and R. Ghaffari. Chaotic dynamics of an impact oscillator. *Phys. Rev. A*, 27:1741–1743, 1983.
- [23] M.G. Thompson, S.R. Bishop, and S. Foale. An experimental study of low velocity impacts. *Machine Vibration*, 3:10–17, 1994.
- [24] C.A. Van Eysden and J.E. Sader. Frequency response of cantilever beams immersed in compressible fluids with applications to the atomic force microscope. *J. Appl. Phys.*, 106:art.no. 094904, 2009.

- [25] C.P. Vyasarayani, J. McPhee, and S. Birkett. Modeling impacts between a continuous system and a rigid obstacle using coefficient of restitution. *Journal of Applied Mechanics*, 77(2):021008, 2010.
- [26] D.J. Wagg. A note on using the collocation method for modelling the dynamics of a flexible continuous beam subject to impacts. *J. Sound Vib.*, 276(3-5):1128–1134, 2004.
- [27] D.J. Wagg. A note on coefficient of restitution models including the effects of impact induced vibration. *J. Sound Vib.*, 300(3-5):1071–1078, 2007.
- [28] D.J. Wagg and S.R. Bishop. Application of non-smooth modelling techniques to the dynamics of a flexible impacting beam. *J. Sound and Vib.*, 256, 2002.
- [29] D.J. Wagg, G. Kapondinis, and S.R. Bishop. An experimental study of the impulse response of a vibro-impacting cantilever beam. *Nonlinear Dynam.*, 228(2):243–264, 1999.
- [30] X. Zhao and H. Dankowicz. Characterization of intermittent contact in tapping-mode atomic force microscopy. *ASME J. Comput. Nonlin. Dynam.*, 1:2:1–8, 2006.